Millimeter Wave Systems for Airports and Short-Range Aviation Communications: A Survey of the Current Channel Models at mmWave Frequencies

Mahfuza Khatun[†], Hani Mehrpouyan[†], David Matolak[‡], Ismail Guvenc[♯],

[†] Department of ECE, Boise State University
[‡] Department of Electrical Engineering, University of South Carolina
[♯] Department of ECE, North Carolina State University

email: mahfuzakhatun@u.boisestate.edu, hani.mehr@ieee.org, matolak@cec.sc.edu, iguvenc@ncsu.edu

***Abstract*—Millimeter-wave (mmWave) communications will play a key role in enhancing the throughput, reliability, and security of next generation wireless networks. These advancements are achieved through the large bandwidth available in this band and through the use of highly directional links that will be used to overcome the large pathloss at these frequencies. Although the terrestrial application of mmWave systems is advancing at a rapid pace, the use of mmWave communication systems in aviation systems or airports is still in its infancy. This can be attributed to the challenges related to radio technology and lack of development, and characterization of mmWave wireless channels for the aviation field and the airport environment. Consequently, one of our goals is to develop methodologies that support mmWave air to ground links, and various links at airports, by applying new localization schemes that allow for application of highly directional links that can be deployed over longer distances despite the high path loss at mmWave frequencies. However, a very thorough understanding of the mmWave channel models are needed to enable such new applications. To this end, in this paper, we present a survey of the current channel models in the mmWave band. The 3-dimensional statistical channel model is also reviewed and its parameters and typical characteristics for this model are identified and computed through simulation for the Boise metropolitan area.**

I. Introduction

Wireless systems are increasingly supporting larger and more diverse applications from sensor networks for environmental monitoring, to "smart grid" electrical infrastructures, to advances in medicine and transportation. To meet this demand, cellular providers need to have access to more bandwidth, which is their primary capital expenditure. They could reduce such costs—and introduce potentially far reaching improvements to cellular access, affordability, and coverage—by making better use of available spectrum in the 30–300 GHz millimeter-wave (mmWave) band [1]. However, propagation and hardware challenges, such as large path loss [2], [3], severe shadowing [2], [3], amplifier limitations [4], [5], [2], phase noise [6], [7], [8], and large power consumption by high speed digital signal processing units (analog-to-digital and digital-to-analog converters) [7], [2], [3], have prevented this.

Quantitative analysis of wireless communication systems requires accurate knowledge of the channels over which the systems will operate. System designs rely on accurate models for these channels. Due to the relative immaturity of channel models for mmWave communication, some assumptions need to be made regarding the channel parameters such as carrier frequency, bandwidth, and mobile unit speed. The main objective of this paper is to present several different mmWave channel models that are under consideration and which are applicable in a wide variety of scenarios. Since the airport and UAV air-ground (AG) channels are not yet quantified, and are in fact a goal of a technical challenge in our NASA ULI project, this paper will only connect the existing models to how they may pertain to our aviation settings.

One of the most recent channel models for the mmWave band has been developed by the group from the New York University (NYU) Polytechnic School of Engineering. Their model is a statistical 3-D omnidirectional channel model. In this work, spatial and temporal models have been developed for 28 GHz outdoor non-line of sight environments [9]. These environments are primarily large cities. This statistical spatial channel model (SSCM) was developed by measuring power delay profiles (PDPs) and from propagation delays estimated from companion ray-tracing models. Power delay profiles are essentially the channel's power output vs. delay when an impulse is put through the channel. The SSCM considers some important parameters such as temporal multipath delays, multipath powers, angle of departure (AOD), and angle of arrival (AOA) information. The SSCM is run using MATLAB(R), enabling the statistical simulator to create mmWave temporal and spatial channel coefficients which, in turn, provide the channel impulse response [9]. Another team from NYU has published work on the same model, but in this case they showed validating experimental measurements and empirically-based channel models for several bands: 28, 38, 60, and 73 GHz [10].

In 2014 the Federal Communications Commission (FCC) gave a Notice of Inquiry (NOI) for technological developments, frequency, performance, and coverage information of mmWave bands [11]. Most importantly, the FCC requested comments on bands above the 24 GHz frequency spectrum, which includes the mmWave bands. Many corporations and research centers responded to these inquires and began work on mmWave band channel models. The same type of commentary was also found in the UK's Ofcom in 2015 [12]. In late 2014, Samsung researchers declared that they had developed the world's first high-speed data rate link transmitting 1.2 Gbps, or 150 MB per second, on a highway at over 100 km/h by

using a 28 GHz band wireless link. Samsung's research showed a significant step towards the utilization of mmWave bands based on 3-D channel models [13]. However, to date there are very few results and essentially zero channel models in the mmWave band for air to ground settings.

Accordingly, one of our primary efforts in the proposed project will be to develop accurate, empirically-based mmWave channel models for two key applications: the airport surface area, and short-range air-ground links. These models will be validated by measurements and compared to existing mmWave models in the literature, as well as compared with results from ray-tracing simulations using the WinProp(R) and Wireless InSite(R) software in these environments. The other primary effort is to develop novel, tailored waveforms and medium-access data link layer (DLL) protocols suitable for reliable mmWave networking. The channel models will include the use of multiple antennas for the high capacity mmWave AG links, and multiple mmWave bands. For the airport applications, since many tenants, e.g., airlines, airport authorities, local security, require highly reliable and secure data transfer, but at low data rates, novel PHY/DLL designs (including direct-sequence and frequency-hopped spread spectrum, high-order frequency shift keying) will be investigated in conjunction with spatial and site diversity to ensure resilience to obstructions.

Although the above work is underway, at this point in the project, we find it appropriate to provide a survey of the current mmWave channel models. Accordingly, this paper is organized as follows: In Section II we present some summary remarks regarding mmWave channel models, Section III is an in-depth look at the 3-D statistical channel model, Section IV presents the simulation results of the SSM mmWave channel model in the city of Boise. Finally, Section V concludes this paper and has remarks about future work.

II. General Remarks on mmWave Channel models

For mmWave communication, as with other bands, channel models are an important tool. There are three main types of channel models available: statistical, site specific (deterministic), and a combination of these two approaches. The complexity and size of the parameters associated with a channel model depend on the desired bandwidth, setting, and "portability," or ability to serve in settings other than those from/for which the model was developed.

In this paper, we include results from recent and published channel models for mmWave bands for both non-line-of-sight[1] (NLOS) and line-of-sight (LOS)[2] environments.

Since mmWave links are expected to be used for relatively large data rates, channel bandwidths will be larger compared to that of current systems, e.g., Long Term Evolution (LTE). On the other hand, significant path loss and shadowing continue to barriers to achieving higher throughputs. On the other hand, one can utilize highly directional antennas, multi-input multi-output systems and beamforming to reduce the effect of pathloss. Moreover, the multipath components (MPCs) need to be considered for an accurate mmWave channel model, and the parameters for these MPCs, e.g., amplitude, phase, delay, must also be characterized [14].

Taken together, all MPCs make up the channel's impulse response, which is a complete description of any linear and time-varying channel. Since mmWave band signals also incur large attenuation (spreading or basic transmission loss) directional antennas may be required for maintaining a reliable link between the transmitter and receiver. The use of directional antennas requires the estimation of AOD and AOA also. Finally, here, as in models for lower frequency bands, aggregate channel attenuation, or path loss, is also critical from a link planning perspective. Hence, models for mmWave channel path loss are also important.

III. Statistical Channel Model for the mmWave Band

Statistical representations of mmWave propagation channels are promising since their development provides a strong physical basis for development of more accurate and predictive channel models. Statistical models recreate thousands of PDPs from statistical data. Previous research is based on 3-D SSCM for the 28 GHz and the 73 GHz frequency bands [9], [15]. Moreover, there are prior results for the 2-D channel model for the mmWave band in [16].

Let us present the statistical channel impulse response by $h(t, \Theta, \Phi)$, which depends on the multipath AOA, azimuth, and elevation, angles for the received signals, i.e., $\Theta = (\theta, \phi)$, and the AOD, azimuth, elevation angles $\Phi = (\theta, \phi)$. Moreover, here, t, denotes the propagation delay time [9]. The information of AOA and AOD varies with differing environments, i.e. indoor, outdoor. The SSCM channel model provides power relationships that are dependent on the AOA, the AOD, and the time clusters in 2-D and 3-D planes based on the frequency of operation. The total received powers can be found by integrating the PDPs over time.

In the following subsections, we provide the specific components that make up the statistical channel model in the mnmWave band.

A. Path Loss Models

Path loss models are important for calculating the received signal power, i.e., average power over small-scale and large-scale fading. These models depend on distance, wavelength, bandwidth, antenna height, building height, and environmental variables. The total omnidirectional power is measured using a free space path loss model with consideration for the shadowing factor, AOA, and AOD [17].

Important characteristics for path loss models are the path loss exponent and the shadowing factor, which change for both LOS and NLOS transmissions. Moroever, the antenna height

[1]Non-line-of-sight represents the scenario when a large obstruction–large with respect to a wavelength–exists between transmitter (TX) and receiver (RX). A NLOS with moderate obstruction is when there exists some foliage between transmitter and receiver or when the receiver is just slightly behind a large object, where the first Fresnel zone is not fully blocked. Finally, for directional links, NLOS refers to the case when antennas are not aligned.

[2]When no obstruction exist between the transmitter and receiver antennas. If antennas are directional, they are pointed directly toward each other, i.e., aligned in both azimuth and elevation.

and the use of directional or omni-directional antennas also affect the shadowing factor. When considering a dense urban NLOS environment, in [9], the authors show that the path loss exponent and shadowing factor are 3.4 and 9.7, respectively, for the 28 GHz band when using omnidirectional antenna . The same authors published a 28 GHz and 73 GHz channel model based on the free space path loss model, which included both omnidirectional and directional antennas in LOS and NLOS environments [18]. In addition, the close-in (CI) free space path loss model was selected for its simpler form and physical basis, which is also claimed to be more accurate for mmWave frequencies [10].

Let us present the CI pathloss mode byl [17]

$$PLM(d) = PLM(d_o) + 10n \cdot \log_{10} \frac{4\pi d}{\lambda} + \chi_\sigma \quad (1)$$

$$PLM(d_o) = 20 \log_{10} \frac{4\pi d}{\lambda} \quad (2)$$

where, n is the path loss exponent, λ is the carrier wavelength, χ_σ is a log-normal random variable with 0 dB mean and standard deviation σ, and $d_o = 1m$. The CI model provides variation for both LOS and NLOS power statistics at mmWave frequencies, and is similar to exiting 3-GPP models. The CI model does not change the other model coefficients at various mmWave frequencies. However, recent work vary the path loss exponent, n, with the carrier frequency [15] . A summary of path loss exponent and shadowing factors from different environments for the mmWave band are given in Table I.

TABLE I: Comparison of path loss parameters in different environments of recent works

Ref no	Eenvironment	Freq,GHz	pathloss exponent	shadow factor, dB
[9]	NLOS	28	3.4	9.7
[18]	LOS	28	2.1	3.6
[18]	NLOS	73	3.3	7.6
[18]	LOS	73	2.0	5.2

Finally, it is important to mention that in [13] using the 3D ray-tracing approach, a new dual-slope path loss model has been proposed for the 28 GHz mm-Wave band. Based on four parameters of channel model, the dual-slope is modeled for large-scale channel statistics like path loss and shadowing. The dual-slope model is proposed when the distance between the receiver and transmitter is larger than a pre-determined threshold distance. In the dual-slope model the threshold distance is calculated to reduce the root-mean-square error with respect to measurements [13]. The remaining channel statistics like delay spread and angular spread are determined using the ray-tracing approach for both the urban micro (UMi) and urban macro (UMa) scenarios. The results in [13] show that the dual-slope approach reduces the RMS error with respect to existing path loss models in both UMa and UMi scenarios.

B. Temporal and Spatial Components

The SSCM model is designed with two vital parameters, i.e., the temporal and the spatial statistical parameters. Both parameters are needed for the SSCM 2-D and 3-D models [9]. The temporal component determines the arrival of a group of several MPCs that simultaneously reach the receiver both in time and space. On the other hand, the spatial components takes into account the statistics of both departing and arriving rays over both the azimuth and/or elevation planes. Both of these statistics are explained in detail in [17]. One important information is observed that several time clusters arrive in excess time delay which is several hundreds of nanoseconds at a high gain (24.5 dBi) antenna [9].

1) Time Cluster Power and Intra-Cluster Subpath Power: The relationship between inter-cluster void interval and number of time clusters in PDPs is a concept based on the number of intra-cluster subpaths that occupying less power, while only a few time clusters get a large part of the total received power [9], [19]. Here, we present the results in [9], where the the model is developed with a 25 ns minimum inter-cluster void interval. Figure 1(a) represents the measured temporal cluster power, normalized by the received power in the PDP profile. In this work, the average cluster power, P_o is measured to be 88.3% in the y-intercept at $\tau = 0$ns. The work measured the average cluster decay constant to be $\Gamma = 49.4$ ns. The intra-cluster subpath power (normalized by the cluster power) is plotted against the cluster excess delay time in Figure 1(b). The authors measured the y-intercept of $P_o = 0.342$ and average cluster decay constant of $\gamma = 16.9$ ns.

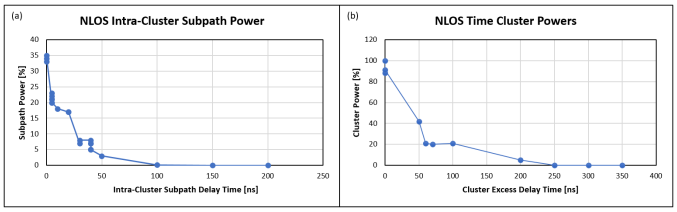

Fig. 1: (a) Measured cluster power normalized by overall received power versus cluster excess delay time, (b) Measured temporal intra-cluster subpath power normalized by overall received power versus intra-cluster subpath excess delay time [9].

2) Comparable Results of RMS Delay Spreads: RMS delay spread is a vital characteristic for accurate channel modeling. In two ways RMS delay spread is calculated [20]. Table II compares the simulated and measured results based on RMS delay spreads for omnidirectional LOS and NLOS scenarios within the bands ranging from 28-73 GHz [15] and the RMS delay spreads statistically for onmidirectional NLOS channels at 28 GHz [9]. In both cases, only few data samples from simulated results break the trend from the measured results. In this case, median value is an important parameter and is considered to change the distribution of the data. At 28 GHZ and considering a NLOS scenario, the medians for the empirical and simulated cases were 31 ns and 32 ns, respectively. These are also close to the measured values [9]. Similarly, the results in [9] present a good match for both thr NLOS and the LOS scenarios at the 73 GHz band [15].

TABLE II: A comparable table of 28 GHz and 73 GHz omnidirectional RMS Delay Spreads - CDF

Ref. no	Frequency, GHz	Scenario	Methodology	Median, ns	Probability, %
[2]	28	NLOS	Simulated	32	Good
			Measured	31	
[7]	Combined 28-73	NLOS	Simulated	32	Good
			Measured	31	
		LOS	Simulated	16	Good
			Measured	18	

C. Cluster Decay Model

The cluster decay model is important for calculating cluster power in mmWave communications, which is comprised of an extended Saleh-Valenzuela model. In [21] the authors analyze the cluster decay and fading for indoor mmWave channel where noise floor was taken into consideration. In this work the authors estimated the parameters for 700 samples based on measurement and synthetic data. Taking reference noise floor at $\ln(P_{noise}) = -24$dB, the cluster decay is more accurate for truncated regression in comparison to non-truncated regression data as shown in [21]. Based on the measurement data at 62 GHz in an indoor environment the noise power is estimated at -27.1 dB. The data contains both LOS and obstructed line-of-sight (OLOS) scenarios and these components are assumed to be the same as the cluster decay and fading parameters [21]. Based on the cluster delay parameters for both truncated and non-truncated data, two different power-delay-profiles (PDFs) are created by the stochastic channel model [22]. The PDP channel model for estimation of non-truncated data are close to the measured data as seen in [21]. The authors also represented that, if the noise power is not taken into consideration, the RMS delay spread for non-truncated regression model is estimated to play a more important role compared to the truncated regression model for both LOS and OLOS [21].

IV. Simulation of 3-D SSCM Models

The simulation of the selected model with different choice of parameters is carried out in this section. It should be noted that statistical channel modeling is focused on extracting models form the measured azimuth and elevation power spectrum using 3-D ray-tracing predictions and generating the required data when measurements are not available [23]. For the simulation, assumptions were made for both channel and antenna properties, which can be seen in Table III and Table IV.

To simulate a NLOS environment within the Boise metropolitan and surrounding areas, channel parameters were generated to match the average environmental variables. For example, the average barometric pressure in the Boise area is 1020 mbar, the average temperature is 11.39°C, and average humidity is set to 55%. Combined with the channel parameters for 5G, the frequencies simulated were 28 GHz and 73 GHz with an RF bandwidth of 800 MHz. For an average user, the transmitter to receiver separation were set to 10 - 500 m with an (ideal) co-polarization reception angle.

The antenna parameters used were set to standard values so that simulations remained constant and independent of antennas. The TX and RX array types were set to URA for higher throughput, in accordance with [24]. Antenna spacing was set to 0.5λ so that there was no chance for a receiving party to be out of range and the azimuth and elevation were set at 10° so that both azimuth and elevation beams could be used.

A. AOA and AOD Lobe Power Spectrum

The AOA and AOD lobe power spectra reveal that between the 28 GHz and 73 GHz simulations, we see a similar power level. The multipath power delays were seen to be a function of the azimuth angle for both TX and RX. The received power is plotted into polar plots for both the 28 GHz and 73 GHz frequencies bands as shown in Figures 2, 4 and Figures 3, 5, respectively. Each ray represents the peak of a lobe[3], where each lobe represents a possible propagation route.

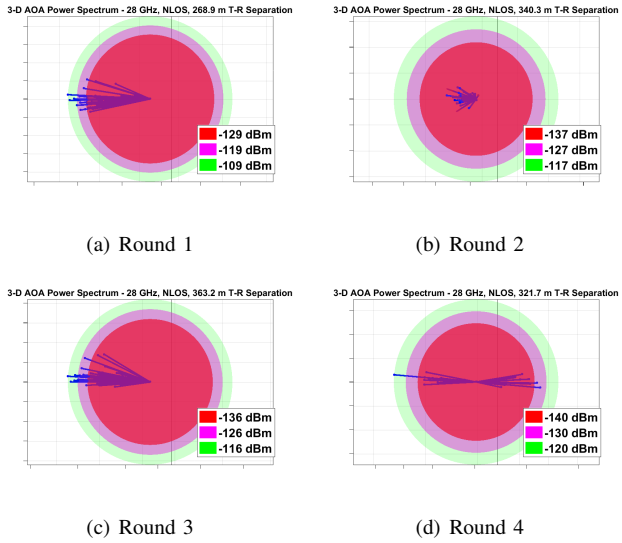

(a) Round 1 (b) Round 2

(c) Round 3 (d) Round 4

Fig. 2: AOA Lobe Power Spectrum for 28GHz, 30dBm.

AOA and AOD can be defined as $\bar{\Theta}$ which represents a power-weighted mean pointing angle (angle of direction). $\bar{\Theta}$ can be used on each lobe to identify a single direction of energy arrival/departure calculated by ,

$$\bar{\Theta} = \frac{\sum_k P(\Theta_k)\Theta_k}{\sum_k P(\Theta_k)} \tag{3}$$

where k is the index of the pointing angle, in degrees, within a lobe and $P(\Theta_k)$ is the received power at Θ_k. Being that the results and values for both sets of data are randomly generated for differing distances, it is possible for a scenario to be precisely simulated using the 3-D SSCM. The mean value for a set of AOA/AOD rays, i.e. lobes, if measured or simulated in/for a surrounding area should return a uniform distribution between 0 to 360 degrees. As shown by Figures 2, 3, 4, and 5, the AOA/AOD lobe power spectra appear similar and closely

[3]A graphical representation of a contiguous spread of energy arriving or departing the azimuth and elevation planes.

TABLE III: Channel Simulation Parameters

Freq.	RF BW	Scenario	LOS/NLOS	T-R Separation	TX Pow.	Num. RX	Press.	Humidity	Temp.	Pol.
28GHz and 73GHz	800MHz	UMi	NLOS	10m-500m	30dBm	5-10	1020mbar	55%	11.39°C	Co

TABLE IV: Antenna Simulation Parameters

TX/RX Array Type	Num. TX/RX Elements	TX/RX Antenna Spacing	TX/RX Elevation/Azimuth
URA/URA	1/1	0.5λ/0.5λ	10°/10° 10°/10°

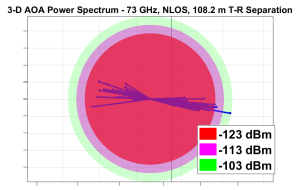

(a) Round 1

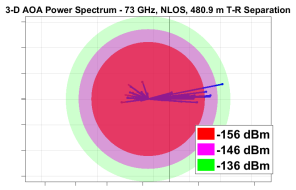

(b) Round 2

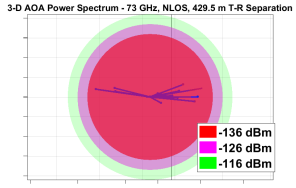

(c) Round 3

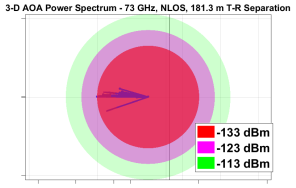

(d) Round 4

Fig. 3: AOA Lobe Power Spectrum for 73GHz, 30dBm.

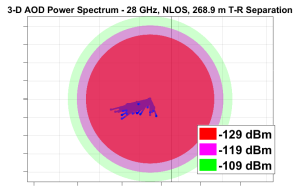

(a) Round 1

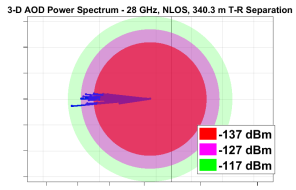

(b) Round 2

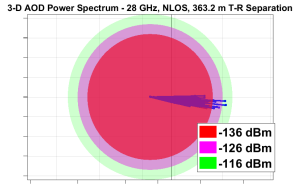

(c) Round 3

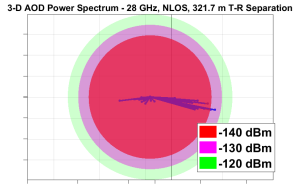

(d) Round 4

Fig. 4: AOD Lobe Power Spectrum for 28GHz, 30dBm.

related. The similarities in power spectra can be attributed to the transmitted power which is set to 30 dBm for all cases, and is not dependent on the frequency of transmission.

B. Omnidirectional PDP

In order to fully understand the channel, the propagation of the channel needs to be examined. Most usually, the propagation is described by the superposition of multiple traveling waves, where each impinging wave at the receiver is described by its path amplitude (voltage), delay, AOD, and AOA. From these components, a double-directional, i.e. omnidirectional, time-invariant channel impulse response (CIR) can be calculated according to [25],

$$h_{omni}(t,\bar{\Theta},\bar{\Phi}) = \sum_{k=1}^{N} a_k e^{j\theta_k}\delta(t-\tau_k)\cdot\delta(\bar{\Theta}-\bar{\Theta}_k)\cdot\delta(\bar{\Phi}-\bar{\Phi}_k) \tag{4}$$

where a_k, θ_k, and τ_k are amplitude, phase, and propagation delay, respectively, of the k^{th} multipath component, $\bar{\Theta}_k$ and $\bar{\Phi}_k$. N represents the total number of of resolvable path components, and $\delta()$ is the Dirac-delta function. For this simulation, the phases and transmission distances are randomized for several runs which can be seen from previous AOD and AOA figures.

While Equation (4) represents an omnidirectional transmitter, there are also several instances where directional transmitters or beam-forming are used for real-world applications. This simulation does include some results for this but, they will not be analyzed in this paper. If one wishes, directional CIR with fixed or arbitrary TX and RX antenna beam positioning can be expressed similarly to Equation (4), except that $\bar{\Theta}$ and $\bar{\Phi}$ need be replaced with the fixed beam positioning values, along with $\delta()$ being replaced with the 3-D azimuth and elevation of complex amplitude antenna patterns being used [26].

Figures 6 and 7 show the resultant calculation and simulation of the omnidirectional power delay profile from (4) for both the 28 GHz and 73 GHz bands. The individual spikes separated on the images represent the superimposed PDP of five individual receptions from different AOAs at the same RX location. The multipath signals earlier in the spectrum arrive before those of the next corresponding AOA. The absolute propagation times were calculated in simulation by using ray-tracing, thus, allowing for alignment with absolute timing of multipath signals originally generated for reception (RX),

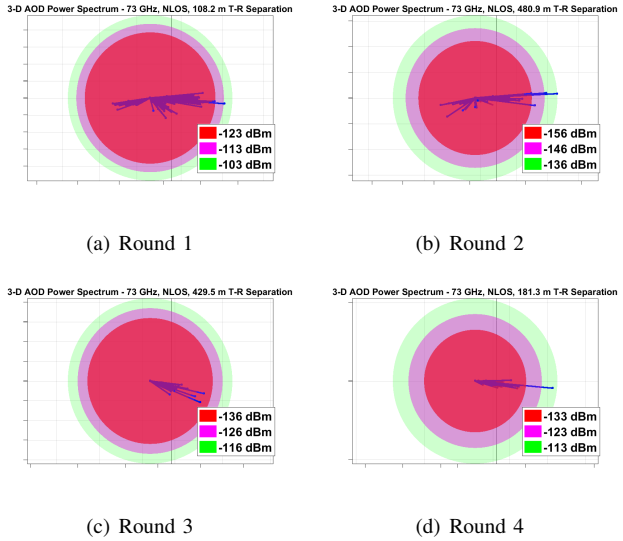

(a) Round 1 (b) Round 2

(c) Round 3 (d) Round 4

Fig. 5: AOD Lobe Power Spectrum for 73GHz, 30dBm.

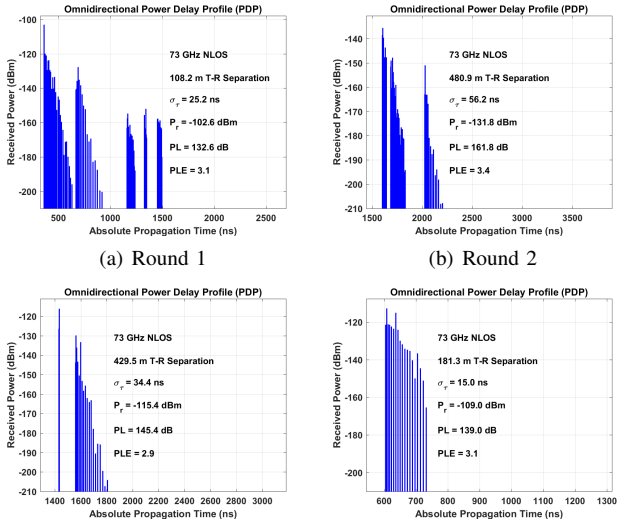

(a) Round 1 (b) Round 2

(c) Round 3 (d) Round 4

Fig. 7: Omnidir. Power Delay Profile for 73GHz, 30dBm.

independent of AOAs [19].

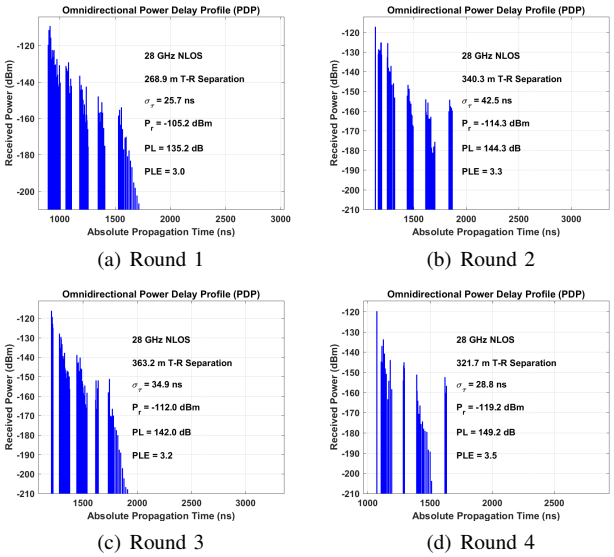

(a) Round 1 (b) Round 2

(c) Round 3 (d) Round 4

Fig. 6: Omnidir. Power Delay Profile for 28GHz, 30dBm.

The 28 GHz and 73 GHz bands proved to be similar in their propagation delays due to their relatively similar separation distances. As separation distances were increased in simulation, the absolute propagation time also increased. The slight differences in attenuation can be noted between the two frequency bands, and it is suspected that, according to [27], a shadowing factor may have come into play which indicated more variability in shadowing at higher mmWave frequencies. The increased shadowing effect can be attributed to increased diffuse scattering, diffraction loss, and weaker reflections.

C. Path Loss

From (1) and (2), along with other research in [28], and [29], path loss can be derived to include dependence on frequency as

$$\overline{PLM(d_o, f)}(dB) = \alpha + \bar{\beta} \cdot 10log_{10}(d_o) + \gamma \cdot 20log_{10}\left(\frac{f}{f_c}\right) \quad (5)$$

where γ represents a frequency dependency factor, and f/f_c is the ratio of frequency deviation from the carrier frequency. $\bar{\beta}$ represents an extracted best-fit linear regression to (5) using path loss values which are computed from the previous section's PDPs by integrating each point to obtain received signal power at each location and AOD, then normalizing to the transmitted power of 30 dBm. The approach used to calculate $\bar{\beta}$ can be described by

$$\bar{\beta} = \frac{\sum_i^n (d_i - \bar{d}_o) \times (PLM_i - \overline{PLM})}{\sum_i^n (d_o - \bar{d})^2}, \quad (6)$$

which is an adaptation of the work found in [30] where d_i is the distance (in dB scale) of the i^{th} measurement of PDPs for a given AOD and RX location. $\bar{d}_o$ is the average distance for all d_i from the simulated value, and $\overline{PLM}$ is the average path loss for the data set. Moreover, here, α represents a floating intercept, as described by [30], of the linear regression fit for (2) and, thus, (5), which can fit data through examination, determines an attenuation point that can be used for the path loss model. α can be determined by

$$\alpha(dB) = \overline{PLM}(dB) - \bar{\beta} \cdot \overline{10log_{10}(d_o)}. \quad (7)$$

For the linear regression, the value for α and $\bar{\beta}$ are solved in parallel form (6) and (7). The regression fit has been computed

for both the set of five transmissions on the 28 GHz and 73 GHz frequencies. Figures 8 and 9 show the path losses for the small set computed. Should a larger set be computed, these results would be more accurate.

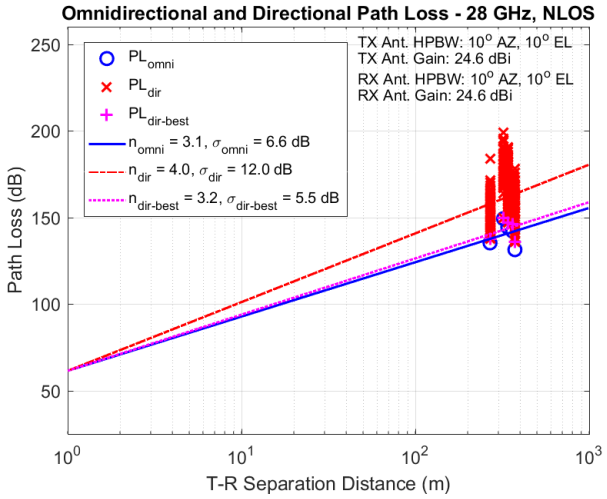

Fig. 8: Path-Loss for 28GHz, 30dBm.

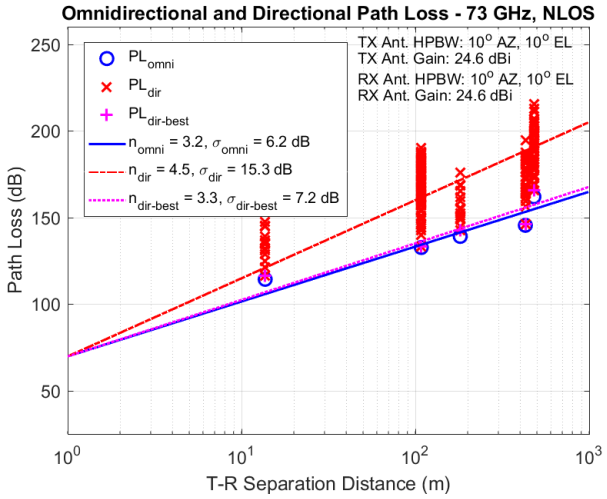

Fig. 9: Path-Loss for 73GHz, 30dBm.

V. Acknowledgment

This work is sponsored by NASAs Aeronautics Research Mission Directorate under the University Leadership Initiative. We would also like to acknowledge our co-investigators, Paul Davis and Benjamin Boisvert at Architecture Technology Corporation. The authors would also like to thank Prof. Theodore Rappaport for providing us with the software to generate the results presented in this paper.

VI. Conclusion

This paper presents the overview of the existing channel models for mmWave bands. Initially, the paper address the outcomes and findings corresponding to the channel models from the recent works. Next, the simulation results of 3-D statistical channel models is included for mmWave NLOS communications within the city of Boise. Based on channel parameters, the simulation is successfully completed and the statistics are shown for power lobe AOA/AOD spectra, power delay profiles, and pathloss models for both 28 GHz and 73 GHz bands. Directional and omnidirectional path loss models were both presented with respect to a random sample of 10 to 500 m distances. For path loss models, the exponential value is similar for both the 28 GHz and 73 GHz omnidirectional transmissions. The antenna parameters are kept the same for all cases in simulation.

The 3-D statistical channel and pathloss models are able to provide assistance in the development of systems and their analysis for next-generation 5G mobile networks. Hopefully, by 2020, both the 28 GHz and 73 GHz frequency bands will be implemented in 5G technology to provide higher data rates and spectral efficiency.

References

[1] A. Osseiran, F. Boccardi, V. Braun, K. Kusume, P. Marsch, M. Maternia, O. Queseth, M. Schellmann, H. Schotten, H. Taoka, H. Tullberg, M. A. Uusitalo, B. Timus, and M. Fallgren, "Scenarios for 5G mobile and wireless communications: The vision of the METIS project," vol. 52, no. 5, pp. 26–35, May 2014.

[2] T. S. Rappaport, R. W. Heath, R. C. Daniels, and N. Murdock, *Millimeter-Wave Wireless Communications*. Prentice Hall, 2014.

[3] K.-C. Huang and Z. Wang, *Millimeter Wave Communication Systems*. IEEE Series on Digital & Mobile Communication, 2011.

[4] J. J. Yan, C. D. Presti, D. F. Kimball, Y.-P. Hong, C. Hsia, P. M. Asbeck, and J. Schellenberg, "Power amplifiers: Efficiency enhancement of mm-Wave power amplifiers using envelope tracking," *IEEE Microwave and Wireless Components Letters*, vol. 21, no. 3, pp. 157–159, Feb. 2011.

[5] T. Rappaport, J. Murdock, and F. G. Jr., "State of the art in 60 GHz integerated circuits and systems for wireless communication," *Proceed of the IEEE*, vol. 99, no. 8, pp. 1390–1436, Aug. 2011.

[6] S. Suyama, Y. Hashimoto, H. Suzuki, and K. Fukawa, "60 GHz OFDM experimental system employing decision-directed phase noise compensation," Jan. 2012, pp. 191–194.

[7] J. Wells, *Multi-Gigabit Microwave and Millimeter-Wave Wireless Communications*. Artech House., 2010.

[8] H. Mehrpouyan, M. R. Khanzadi, M. Matthaiou, A. M. Sayeed, R. Schober, and Y. Hua, "Improving bandwidth efficiency in E-band communication systems," vol. 52, no. 3, pp. 121–128, Mar. 2014.

[9] M. K. Samimi and T. S. Rappaport, "3-d statistical channel model for millimeter-wave outdoor mobile broadband communications," in *Communications (ICC), 2015 IEEE International Conference on*. IEEE, 2015, pp. 2430–2436.

[10] T. S. Rappaport, G. R. MacCartney, M. K. Samimi, and S. Sun, "Wideband millimeter-wave propagation measurements and channel models for future wireless communication system design," *IEEE Transactions on Communications*, vol. 63, no. 9, pp. 3029–3056, 2015.

[11] R. H. Coase, "The federal communications commission," *The Journal of Law and Economics*, vol. 56, no. 4, pp. 879–915, 2013.

[12] U. Ofcom, "Spectrum above 6 ghz for future mobile communications," 2015.

[13] Y. Chang, S. Baek, S. Hur, Y. Mok, and Y. Lee, "A novel dual-slope mm-wave channel model based on 3d ray-tracing in urban environments," in *Personal, Indoor, and Mobile Radio Communication (PIMRC), 2014 IEEE 25th Annual International Symposium on*. IEEE, 2014, pp. 222–226.

[14] M. Reil and G. Lioyd, "Millimeter-wave beamforming: Antenna array design choices & characterization," *Rhode and Shwartz White Paper*, Mar. 2016.

[15] M. K. Samimi and T. S. Rappaport, "Statistical channel model with multi-frequency and arbitrary antenna beamwidth for millimeter-wave outdoor communications," in *Globecom Workshops (GC Wkshps), 2015 IEEE*. IEEE, 2015, pp. 1–7.

[16] S. Sun, T. S. Rappaport, R. W. Heath, A. Nix, and S. Rangan, "Mimo for millimeter-wave wireless communications: beamforming, spatial multiplexing, or both?" *IEEE Communications Magazine*, vol. 52, no. 12, pp. 110–121, 2014.

[17] G. MacCartney Jr, M. Samimi, and T. Rappaport, "Omnidirectional path loss models at 28 ghz and 73 ghz in new york city," in *2014 IEEE International Symposium on Personal, Indoor, and Mobile Radio Communications (PIMRC)*, 2014, pp. 227–231.

[18] A. A. Saleh and R. Valenzuela, "A statistical model for indoor multipath propagation," *IEEE Journal on selected areas in communications*, vol. 5, no. 2, pp. 128–137, 1987.

[19] M. Samimi and T. Rappaport, "Ultra-wideband statistical channel model for 28 ghz millimeter-wave urban nlos environments," *GLOBECOM2014, Austin, TX USA*, 2014.

[20] A. F. Molisch, "Statistical properties of the rms delay-spread of mobile radio channels with independent rayleigh-fading paths," *IEEE Transactions on Vehicular Technology*, vol. 45, no. 1, pp. 201–204, 1996.

[21] C. Gustafson, D. Bolin, and F. Tufvesson, "Modeling the cluster decay in mm-wave channels," in *Antennas and Propagation (EuCAP), 2014 8th European Conference on*. IEEE, 2014, pp. 804–808.

[22] C. Gustafson, K. Haneda, S. Wyne, and F. Tufvesson, "On mm-wave multipath clustering and channel modeling," *IEEE Transactions on Antennas and Propagation*, vol. 62, no. 3, pp. 1445–1455, 2014.

[23] T. A. Thomas, H. C. Nguyen, G. R. MacCartney, and T. S. Rappaport, "3d mmwave channel model proposal," in *Vehicular Technology Conference (VTC Fall), 2014 IEEE 80th*. IEEE, 2014, pp. 1–6.

[24] N. Moraitis and P. Constantinou, "Indoor channel capacity evaluation utilizing ula and ura antennas in the millimeter wave band," in *Personal, Indoor and Mobile Radio Communications, 2007. PIMRC 2007. IEEE 18th International Symposium on*. IEEE, 2007, pp. 1–5.

[25] M. Steinbauer, A. F. Molisch, and E. Bonek, "The double-directional radio channel," *IEEE Antennas and propagation Magazine*, vol. 43, no. 4, pp. 51–63, 2001.

[26] S. Sun, G. R. MacCartney, M. K. Samimi, and T. S. Rappaport, "Synthesizing omnidirectional received power and path loss from directional measurements at millimeter-wave frequencies," in *2015 IEEE Global Telecommunications Conference (GLOBECOM 2015)*, 2015, pp. 3948–3953.

[27] G. R. MacCartney, T. S. Rappaport, S. Sun, and S. Deng, "Indoor office wideband millimeter-wave propagation measurements and channel models at 28 and 73 ghz for ultra-dense 5g wireless networks," *IEEE Access*, vol. 3, pp. 2388–2424, 2015.

[28] J. Keignart, J. Pierrot, N. Daniele, A. Alvarez, M. Lobeira, J. Garcia, G. Valera, and R. Torres, "Ucan report on uwb basic transmission loss," *Tech. Rep. IST-2001-32710 UCAN*, 2003.

[29] S. Piersanti, L. A. Annoni, and D. Cassioli, "Millimeter waves channel measurements and path loss models," in *Communications (ICC), 2012 IEEE International Conference on*. IEEE, 2012, pp. 4552–4556.

[30] N. L. Johnson, S. Kotz, and N. Balakrishnan, *Discrete multivariate distributions*. Wiley New York, 1997, vol. 165.